Journal of Alloys and Compounds 509 (2011) 9127–9132

Contents lists available at ScienceDirect

Journal of Alloys and Compounds

journal homepage: www.elsevier.com/locate/jallcom

Dielectric investigation of $M^{II}M^{IV}(PO_4)_2$ double orthophosphates (M^{II} = Ca, Sr, Ba, Pb; M^{IV} = Ti, Zr, Hf, Ge, Sn)

Florin Tudorache[a,*], Karin Popa[b,*], Liliana Mitoseriu[a], Nicoleta Lupu[c], Damien Bregiroux[d], Gilles Wallez[d]

[a] Alexandru Ioan Cuza" University of Iasi, Faculty of Physics, no. 11, Carol I Blvd., 700506 Iasi, Romania
[b] Alexandru Ioan Cuza" University of Iasi, Faculty of Chemistry, no. 11, Carol I Blvd., 700506 Iasi, Romania
[c] National Institute of R & D for Technical Physics-IFT, Magnetic Materials and Devices Department, no. 47, D. Mangeron Blvd.,700050 Iasi, Romania
[d] UPMC Univ. Paris 06, CNRS-UMR 7574, Chimie-ParisTech, Laboratoire de Chimie de la Matière Condensée de Paris, 11 rue Pierre et Marie Curie, 75231 Paris Cedex 05, France

ARTICLE INFO

Article history:
Received 25 February 2011
Received in revised form 15 June 2011
Accepted 16 June 2011
Available online 22 June 2011

Keywords:
Double orthophosphates
Crystal structure
Dielectric properties

ABSTRACT

$M^{II}M^{IV}(PO_4)_2$ (M^{II} = Ca, Sr, Ba, Pb; M^{IV} = Ti, Zr, Hf, Ge, Sn) ceramics were prepared by solid state reaction method and consolidated by spark plasma sintering in order to study their electrical properties. The dielectric study performed at room temperature was aimed to determine the basic electrical properties of these compounds. Maxwell–Wagner polarization contributions, which are active at low frequencies cause a strong extrinsic increase of both real and imaginary part of permittivity as well of the dc-conductivity for $BaZr(PO_4)_2$, $BaTi(PO_4)_2$, $BaHf(PO_4)_2$, and $SrGe(PO_4)_2$ double orthophosphates. Moderate real ($\varepsilon'_r = 20$–150) and imaginary low-frequency permittivity ($\varepsilon'_r = 7$–300) and typical Debye relaxation with relaxation time in the range of ms is typical for: $PbHf(PO_4)_2$, $PbZn(PO_4)_2$, and $CaGe(PO_4)_2$. At high-frequency ($f = 10^9$ Hz), the ceramics have permittivities of 2.29÷8.02 and tangent loss of 0.003÷0.153. The compounds $SrGe(PO_4)_2$, $BaGe(PO_4)_2$, $BaZr(PO_4)_2$ and $BaSn(PO_4)_2$ have excellent high-frequency dielectric characteristics, with losses of 3÷6% and permittivity slightly above 2 and are possible candidate as microwave ceramics.

1. Introduction

The chemistry of orthophosphates of bivalent and tetravalent cations was extensively reviewed several times during the last 40 years [1–5]. Even so, this class of compounds continues to be interesting in terms of crystal structure [6–13], anisotropic thermal expansion [7,9], optical [17–20] and thermodynamic [21,22] properties. Thus, most of the inactive $M^{II}M^{IV}(PO_4)_2$ are layered compounds with yavapaiite ($KFe(SO_4)_2$) structure. Than the tetravalent cation is an actinide, $M^{II}M^{IV}(PO_4)_2$ adopts a distorted cheralite ($CaTh(PO_4)_2$) structure. A reversible thermal-induced phase transition of $C2/m$ to $P\bar{3}1m$ was described and characterized during heating and cooling in $BaZr(PO_4)_2$ and $BaHf(PO_4)_2$ compounds [3,9,21,22]. $SrZr(PO_4)_2$ also presents two thermal-induced phase transitions, as revealed by DTA measurement [7].

Double phosphates are considered as promising crystalline matrices for the immobilization of high-level nuclear waste [23–29]. The interest in potential phosphate-based waste form has developed because the high-active waste generated by reprocessing of spent nuclear fuel may contain up to 15 wt.% P_4O_{10} that results from processing technologies that utilize tributylphosphate.

There are a number of studies on the optical properties of such compounds [14–16]. Thus, $BaTi(PO_4)_2$ is yellow-emitting due to the octahedral environment of titanium [17]. $BaHf_{1-x}Zr_x(PO_4)_2$ solid-solutions and the end-members are used in medical imaging with the aim of reducing the exposure of the patient to X-rays while maintaining the structural features of the X-ray image [18] and it were found to be potentially attractive candidate for use in medical diagnosing imaging systems (two-sided mammography screen applications). Due to the high luminescent intensity, excellent color purity and chemical stability, Eu^{III}, Tb^{III} and Tm^{III} doped $CaZr(PO_4)_2$ are attractive red, green and blue emitting X-ray and plasma display panel phosphors [19].

Phosphates were reported to be either excellent dielectric materials, as already demonstrated for other structural classes [30,31], while some compounds have been reported to be ionic conductors [32]. In fact, the dielectric properties of double phosphates were not investigated in detail and no information related to the influence of the composition and microstructural characteristics on the complex dielectric properties are found in the literature for this

* Corresponding authors. Tel.: +40 232 201050; fax: +40 232 201150.
E-mail addresses: florin.tudorache@uaic.ro (F. Tudorache), kpopa@uaic.ro (K. Popa).

0925-8388/$ – see front matter © 2011 Elsevier B.V. All rights reserved.
doi:10.1016/j.jallcom.2011.06.072

Table 1
Experimental details for the synthesis of $M^{II}M^{IV}(PO_4)_2$ phosphates.

Compound	M^{II}-source	M^{IV}-source	Thermal treatments
$CaZr(PO_4)_2$	$CaCO_3$ (99%, Prolabo)	ZrO_2 (99%, Aldrich)	5 h/750 °C, 48 h/1200 °C
$CaGe(PO_4)_2$	$CaCO_3$ (99%, Prolabo)	GeO_2 (99.98%, Alfa Aesar)	12 h/600 °C, 72 h/1050 °C
$SrGe(PO_4)_2$	$SrCO_3$ (99%, Prolabo)	GeO_2 (99.98%, Alfa Aesar)	12 h/600 °C, 18 h/1150 °C
$BaGe(PO_4)_2$	$BaCO_3$ (98%, Aldrich)	GeO_2 (99.98%, Alfa Aesar)	12 h/600 °C, 72 h/1100 °C
$BaTi(PO_4)_2$	$BaCO_3$ (98%, Aldrich)	TiO_2 (99.99%, Aldrich)	5 h/1200 °C, 48 h/1200 °C
$BaZr(PO_4)_2$	$BaCO_3$ (98%, Aldrich)	ZrO_2 (99%, Aldrich)	5 h/1200 °C, 48 h/1200 °C
$BaHf(PO_4)_2$	$BaCO_3$ (98%, Aldrich)	HfO_2 (99.9%, Alfa Aesar)	5 h/1200 °C, 48 h/1200 °C
$BaSn(PO_4)_2$	$BaCO_3$ (98%, Aldrich)	SnO_2 (99.9%, Aldrich)	5 h/1200 °C, 48 h/1200 °C
$PbZr(PO_4)_2$	PbO (>99%, Prolabo)	ZrO_2 (99%, Aldrich)	6 h/600 °C, 5 h/1000 °C
$PbHf(PO_4)_2$	PbO (>99%, Prolabo)	HfO_2 (99.9%, Alfa Aesar)	6 h/600 °C, 5 h/1000 °C

class of compounds. In addition, there is nowadays a high interest to search for new types of ceramics as potential materials for filters for telecommunication industry, sensors and transducers industry, microelectronic industry, wireless communications industry, laser industry (like laser materials and luminophores) and if possible, to have multifunctional properties.

This constituted the incentive for the present study, addressed to investigate $M^{II}M^{IV}(PO_4)_2$ double orthophosphates (M^{II} = Ca, Sr, Ba, Pb; M^{IV} = Ti, Zr, Hf, Ge, Sn) prepared by solid state reaction. In order to consolidate them in dense bodies, spark plasma sintering procedure was chosen for a better densification necessary for determination of the complex dielectric characteristics. Spark plasma sintering is process similar to conventional hot pressing in that the precursors are loaded in a graphite die and a uniaxial pressure is applied during the sintering. However, instead of using an external heat source, a dc-current applied during the whole process (3.3 ms pulses of (0.5÷10) kA intensity) is allowed to pass through the electrically conducting pressure die and through the sample.

Various materials have been compacted by spark plasma sintering, due to the fact that the kinetics of densification and grain growth could be manipulated to yield dense nanocrystalline compacts, fully compacted bodies containing metastable constituent or laminated structures. In the last years, this method also was used as an alternative to the classical sintering procedure in order to obtain highly densified ceramics from powders prepared by various wet chemical methods [33–35]. Due to the reducing atmosphere, high levels of oxygen vacancies in oxide ceramics are normally found. Therefore, to re-equilibrate the oxygen level and avoid grain boundary phenomena contributions, a post-sintering re-oxidation process is commonly employed.

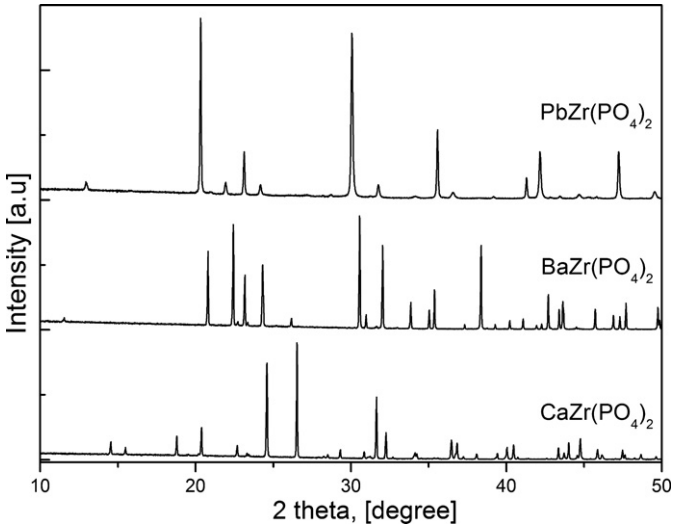

Fig. 1. X-ray diffraction patterns for $PbZr(PO_4)_2$, $BaZr(PO_4)_2$ and $CaZr(PO_4)_2$.

2. Experimental

2.1. Sample preparation and characterization

All the $M^{II}M^{IV}(PO_4)_2$ compounds were obtained by solid state route by thoroughly mixing stoichiometric amounts of M^{II}- and M^{IV}-sources with $NH_4H_2PO_4$ (98.5%, Sigma–Aldrich) under air atmosphere, then heated in alumina crucible. After a preliminary heating treatment aimed to eliminate water, ammonia and carbon dioxide, the mixtures of oxides were ground and submitted to a new thermal treatment. The experimental details, providers and quality of chemicals used for synthesis, are systemized in Table 1.

The obtained powders were further uniaxially pressed into pellets (20 mm diameter, 6÷7 mm thick) and sintered by spark plasma sintering process (FCT-(FAST) HPD-5) for 5 min at 1000 °C and 51 MPa in helium atmosphere, heating and cooling rates: 5 °C/min. Therefore, in order to remove the possible contamination with graphite and to allow the full reoxidation inside the ceramic grains, the pellets were heated for 5 h at 600 °C in air [36]. In order to remove possible contamination with graphite, the pellets were reheated for 5 h at 600 °C in air.

X-ray diffraction (XRD) patterns of all of the powder samples have been recorded on a Panalytical X'pert Pro XRD unit using Cu Kα radiation. The microstructural characterization of the ceramic samples was carried out using a SEM Gemini 1530 microscope.

2.2. Electrical measurements

The electrical measurements were performed on parallel-plate capacitor configuration, by applying Pd–Ag electrodes on the polished surfaces of the sintered ceramic disks, followed by a thermal treatment at 500 °C for 9 h in air. The complex impedance in the low-frequency domain (1 to 10^3) Hz at room temperature was determined by using an impedance bridge type Solartron 1260A Impedance/Gain Phase Analyzer, while the high-frequency complex dielectric properties (10^6 to 10^9) Hz were determined by using an impedance material analyzer type E4991A RF. From the low-frequency impedance spectroscopy data, the dc-conductivity was also estimated, by extrapolation the ac-conductivity to zero frequency, according to the formula: $\sigma_{dc} = \lim_{f \to 0}(2\pi f \varepsilon_0 \varepsilon_r'')$.

3. Results and discussion

All the studied compounds are crystallographically pure, as revealed by XRD analysis (Fig. 1). The crystalline powders were indexed as single phases by using ICDD file numbers $CaZr(PO_4)_2$: 01-073-2816; $CaGe(PO_4)_2$: 00-033-0279; $BaGe(PO_4)_2$: 00-025-0067; $BaTi(PO_4)_2$: 00-025-0081; $BaZr(PO_4)_2$: 00-025-0085; $BaHf(PO_4)_2$: 04-002-9478; $BaSn(PO_4)_2$: 00-025-0078.

The computed cell parameters are shown in the Table 2. As a general trend, it could be observed that most of the inactive double phosphates crystallize in the monoclinic C2/*m* space group (yavapaiite-type compounds, prototype $KFe(SO_4)_2$), as already revealed in [12,37,38]. Exceptions are $CaZr(PO_4)_2$ (orthorhombic), $SrGe(PO_4)_2$ (monoclinic C2/*c* space group at room temperature) and $PbM^{IV}(PO_4)_2$, M^{IV} = Zr; Hf (most likely, hexagonal). Since the crystal structure of $PbZr(PO_4)_2$ and $PbHf(PO_4)_2$ is not yet fully solved, they are not included in Table 2.

The microstructures revealed by the SEM analysis on the fractured ceramic surfaces showed grains with irregularly shaped crystallites: coarse faceted grains with sizes above 5÷10 μm

Table 2
Crystal data of $M^{II}M^{IV}(PO_4)_2$ phosphates and the relative densities of the pellets obtained by spark plasma sintering.

Compound	S.G.	a (nm)	b (nm)	c (nm)	α (°)	β (°)	γ (°)	V (nm^3)	Relative density (%)
$CaZr(PO_4)_2$	$P2_12_12_1$	1.4487	0.6721	0.6234	90	90	90	0.6071	92
$SrGe(PO_4)_2$	$C2/c$	1.6179	0.5067	0.7869	90	115.09	90	0.2909	93
$CaGe(PO_4)_2$	$C2/m$	0.7660	0.5066	0.6992	90	92.59	90	0.2748	94
$BaGe(PO_4)_2$	$C2/m$	0.7952	0.5066	0.7000	90	94.94	90	0.3090	93
$BaTi(PO_4)_2$	$C2/m$	0.8267	0.5184	0.7729	90	94.14	90	0.3304	92
$BaZr(PO_4)_2$	$C2/m$	0.8571	0.5303	0.7887	90	92.99	90	0.3579	92
$BaHf(PO_4)_2$	$C2/m$	0.8539	0.5293	0.7881	90	93.17	90	0.3556	92
$BaSn(PO_4)_2$	$C2/m$	0.8208	0.5239	0.7884	90	94.52	90	0.3380	95

besides small submicron crystallites (dust originating from the polishing process), as presented in the Fig. 2 for $BaM^{IV}(PO_4)_2$ (M^{IV} = Zr, Hf, Sn) ceramics. Similar microstructures were found for all the other compounds. The relative density was about 92÷95% for all the compounds (Table 2).

The frequency dependences of real and imaginary part of permittivity at room temperature for all the $M^{II}M^{IV}(PO_4)_2$ ceramics are presented in the Fig. 3 and the dielectric data are summarized in the Table 3. Two types of samples can be distinguished from the low-frequency properties (below ~10 Hz): (i) compounds with very high real ($\varepsilon'_r = 200 \div 800$) and imaginary low-frequency permittivity ($\varepsilon''_r = 400 \div 3000$): $BaZr(PO_4)_2$, $BaTi(PO_4)_2$, $BaHf(PO_4)_2$, $SrGe(PO_4)_2$, and; (ii) compounds with moderate real ($\varepsilon'_r = 20 \div 150$) and imaginary low-frequency permittivity ($\varepsilon''_r = 7 \div 300$): $PbHf(PO_4)_2$, $PbZn(PO_4)_2$, $BaGe(PO_4)_2$, $BaSn(PO_4)_2$, $CaZr(PO_4)_2$, and $CaGe(PO_4)_2$.

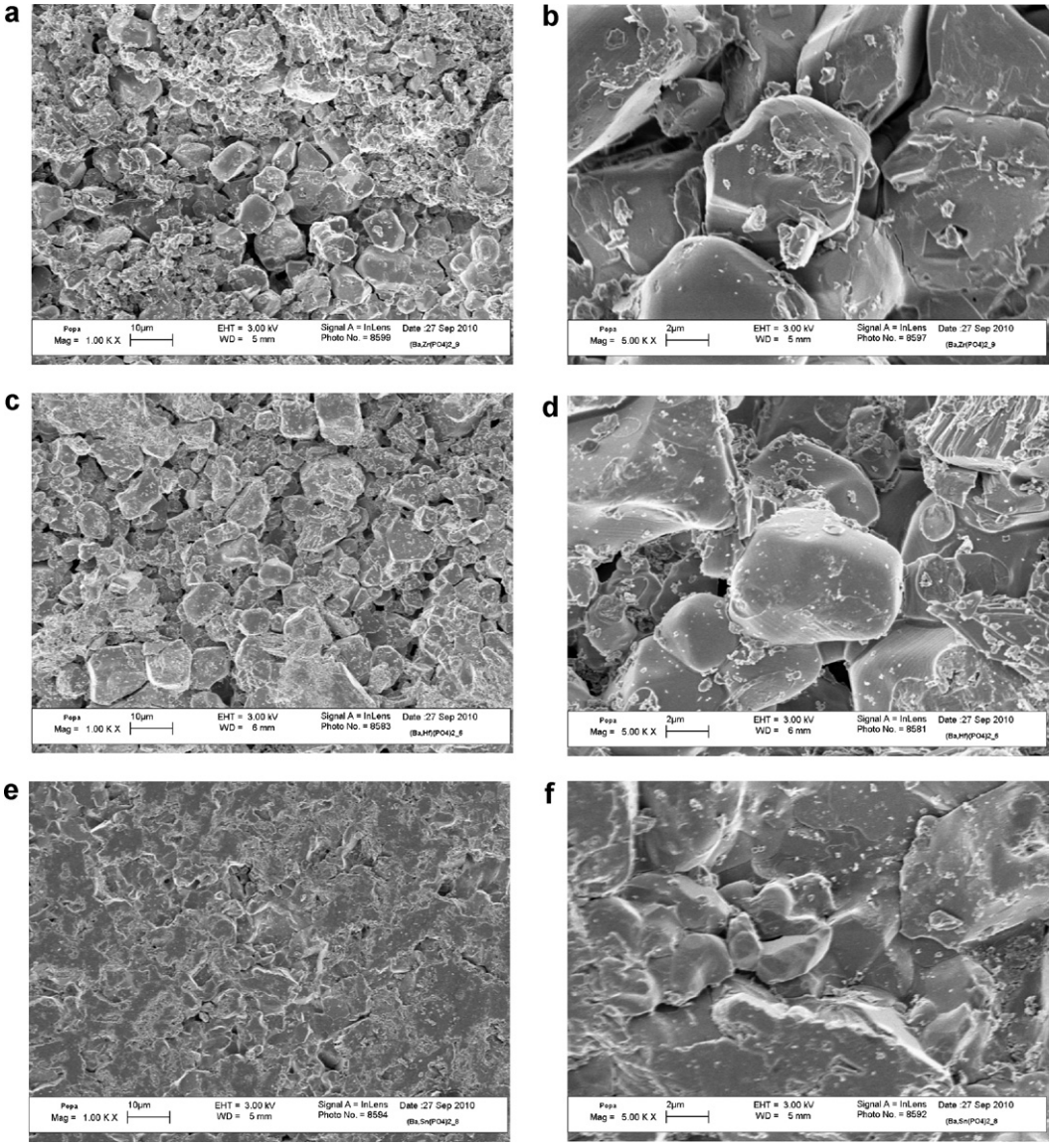

Fig. 2. Typical SEM images of the fractured surface of spark plasma sintered ceramics $BaM^{IV}(PO_4)_2$: $BaZr(PO_4)_2$, ×10,000 (a), ×5000 (b); $BaHf(PO_4)_2$, ×10,000 (c), ×5000 (d); $BaSn(PO_4)_2$, ×10,000 (e), ×5,000 (f) (M^{IV} = Zr, Hf, Sn).

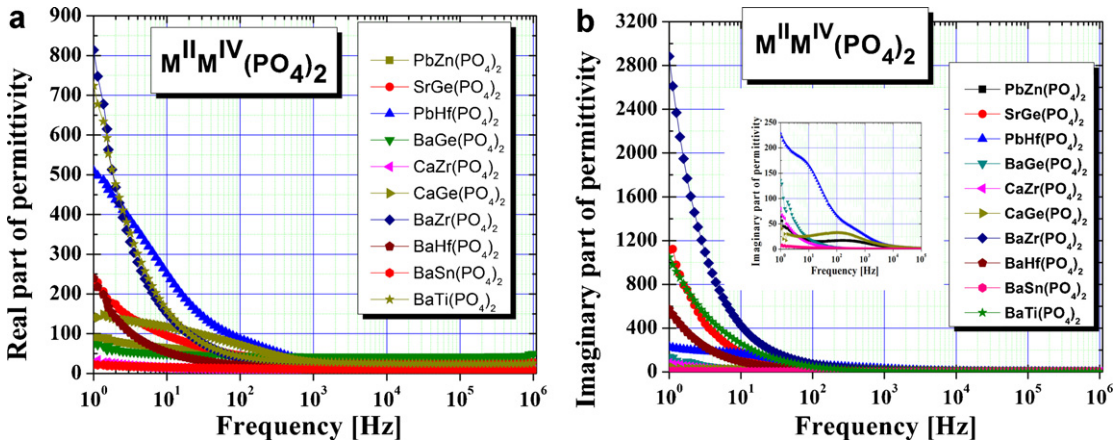

Fig. 3. (a) Real part and (b) imaginary part of permittivity *vs.* frequency at room temperature in $M^{II}M^{IV}(PO_4)_2$ double orthophosphate (M^{II} = Ca, Sr, Ba, Pb; M^{IV} = Ti, Zr, Hf, Ge, Sn) ceramics.

The permittivity of the ceramic material is composed of electronic, ionic, orientation and space charge polarizations. Among them the space charge polarization (Maxwell–Wagner mechanism) [39] depends on the defects of the materials and are dominant in the low-frequency region, while ionic polarization is the main contribution in the microwave frequency region to the permittivity. Thus, the dielectric properties at low frequencies are dominated by very slow species, which are normally charge defects e.g. cation vacancies or local dielectric non-homogeneities like different oxygen stoichiometry at grain boundaries or within the ceramic grain. Such slow charges produce Maxwell–Wagner polarization dispersion, which seems to be mostly active phenomena for the ceramic $BaZr(PO_4)_2$, $BaTi(PO_4)_2$, $SrGe(PO_4)_2$, and $BaHf(PO_4)_2$ compounds and less important in all the other ones. Such properties are related to some microstructural and local compositional heterogeneities in these samples, not related to secondary phases. Once the slow polarization phenomenon is over, above 1 kHz, no other relaxation mechanisms seems to be active for these ceramic compositions, at room temperature.

Among the compositions with low Maxwell–Wagner effect, three compounds ($PbHf(PO_4)_2$, $PbZn(PO_4)_2$, and $CaGe(PO_4)_2$) present a Debye dipolar relaxation with a single-relaxation time τ:

$$\tilde{\varepsilon} = \varepsilon_\infty + \frac{\varepsilon_s - \varepsilon_\infty}{1 + i\omega\tau} \quad (1)$$

where ε_∞ and ε_s are the high-frequency, and the static permittivity, respectively. The Debye relaxation manifests by an inflexion of the real part of permittivity and a maximum of the imaginary part of permittivity in the permittivity-frequency dependences. Among these compounds, the Debye relaxation is overlapped by a weak Maxwell–Wagner space charge effect which manifests at low frequencies (Fig. 3b). However, for all of those compounds the relaxation time can be clearly determined as being in the range of ms: τ = 28 ms for $PbHf(PO_4)_2$, τ = 1.25 ms for $CaGe(PO_4)_2$ and τ = 1.0 ms for $PbZn(PO_4)_2$ and they characterize slow dipolar reorientations or oxygen vacancies-hopping processes commonly present in complex oxide materials [39].

The Maxwell–Wagner effect strongly affects the dielectric loss ($\tan\delta > 1$) and increases the dc-conductivity. The highest value of the dc-conductivity is found for the $BaZr(PO_4)_2$ compound, which has the character of an ionic conductor at room temperature ($\sigma_{dc} \sim 1.60 \times 10^{-7}$ S/m). More relevant dielectric data to be compared at room temperature can be found at f = 1 kHz (Table 3): for all the ceramics investigated in the present study, the permittivity is in the range of ~9.24 for $CaZr(PO_4)_2$ to ~42.56 for $BaGe(PO_4)_2$, while the dielectric losses are in the range of ~0.01÷0.05 for $BaGe(PO_4)_2$ and $CaZr(PO_4)_2$, which are excellent dielectrics, to around unit for $PbHf(PO_4)_2$ and $BaZr(PO_4)_2$, which probably are ionic conductors [7]. Detailed temperature-dependences of the electrical properties, which are beyond the interest of the present work, might clarify the nature of conductivity in such compounds.

The intrinsic dielectric character of $M^{II}M^{IV}(PO_4)_2$ crystallizing in C2/*m* monoclinic space group has its origin most likely in their layered crystal structure [3,9,10], which is not the case of monazites and diphosphates, for instance (Fig. 4). Also $SrGe(PO_4)_2$ and $CaZr(PO_4)_2$ might be regarded as distortions of this structure. Thus, the simplest way to describe such double phosphates is to consider PO_4 tetrahedra isolated in a two-direction array and further interconnected by $M^{IV}O_6$ via corner-sharing oxygen atoms to form $[M^{IV}(PO_4)_2]^{2-}$ anionic bidirectional sheets. The charge is compensated by cationic sheets formed by the big M^{II} cations. Thus, the insulating character results from the sheets staking along the (0 0 1) direction [40].

Table 3
Summary of the dielectrics characteristics of $M^{II}M^{IV}(PO_4)_2$ ceramics.

Compound	Low frequency (10^3 Hz)		High frequency (10^9 Hz)		dc-Conductivity (S/m)
	Real permittivity	Dielectric loss	Real permittivity	Dielectric loss	
$CaZr(PO_4)_2$	9.24	0.05	4.82	0.008	4.47×10^{-9}
$SrGe(PO_4)_2$	30.60	0.24	2.29	0.003	6.19×10^{-8}
$CaGe(PO_4)_2$	27.13	0.68	6.26	0.005	2.58×10^{-9}
$BaGe(PO_4)_2$	42.56	0.01	2.36	0.003	7.58×10^{-9}
$BaTi(PO_4)_2$	29.03	0.27	8.02	0.153	5.81×10^{-8}
$BaZr(PO_4)_2$	14.12	0.97	2.81	0.003	1.60×10^{-7}
$BaHf(PO_4)_2$	10.16	0.49	7.44	0.010	3.17×10^{-8}
$BaSn(PO_4)_2$	11.1	0.06	5.94	0.006	3.37×10^{-10}
$PbZn(PO_4)_2$	18.17	0.70	5.34	0.011	3.60×10^{-9}
$PbHf(PO_4)_2$	26.57	1.04	4.12	0.009	1.27×10^{-8}

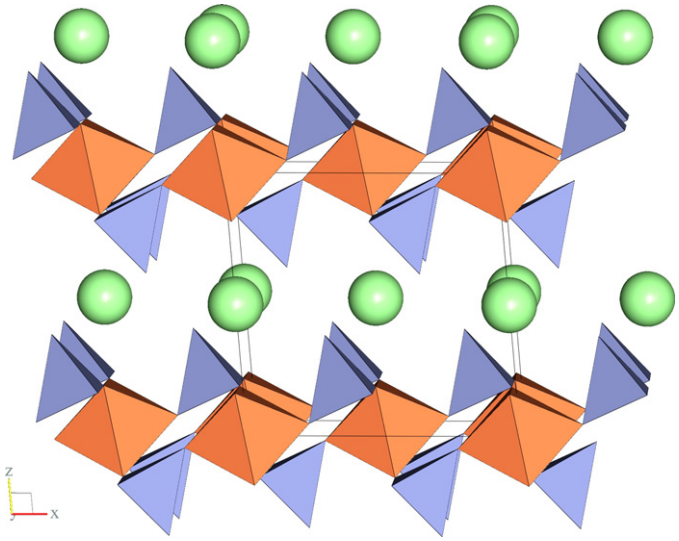

Fig. 4. Crystal structure of $BaM^{IV}(PO_4)_2$ compounds viewed along *b*-axis (M^{IV} = Ge, Ti, Zr, Hf, Sn).

Due to extrinsic contributions to the polarization and permittivity (space charge, grain boundary phenomena, etc.), more relevant information concerning the intrinsic dielectric properties are obtained by measuring their properties at high frequencies. Dielectric measurements in the frequency range of (10^3–10^9) Hz showed that all the investigated ceramics are in that frequency ranges rather good dielectrics (Table 3). At the frequency $f = 10^9$ Hz, the investigated ceramic compounds have permittivities of 2.29÷8.02 and tangent loss of 0.003÷0.153, the highest intrinsic losses being found in $BaTi(PO_4)_2$. $SrGe(PO_4)_2$, $BaGe(PO_4)_2$, $BaZr(PO_4)_2$, and $BaSn(PO_4)_2$ ceramics have excellent high-frequency dielectric characteristics, with losses of 3÷6% and permittivity slightly above 2, while $BaSn(PO_4)_2$ has excellent dielectric properties in the frequency range investigated in the present work, with the smallest dc-conductivity of 3.37×10^{-10} S/m and a rather high permittivity of 11.1 and low losses of 6% at 1 kHz. In overall frequency range very good dielectric properties are also shown by $CaZr(PO_4)_2$ and $BaGe(PO_4)_2$ phosphates (Table 3).

The investigated compounds with good dielectric properties at high frequencies attract a high interest as ceramic materials for microwave applications, for which high quality factors Qxf = *f*/tan δ at microwave frequencies and permittivity in the range of tenths–hundreds are required. The main applications of these ceramics are for dielectric resonators and substrates for high-temperature superconducting (HTSC) microwave devices [41–43], for which the materials should have a low permittivity about 10, to reduce the signal delay time, a high quality factor (Qxf) for frequency selectivity and a low temperature coefficient of resonant frequency for temperature stability. As for other phosphate systems, it is expected that some of the present $M^{II}M^{IV}(PO_4)_2$ compounds would also have a permittivity lower than 10 in the microwave frequency region due to strong covalent bonding in P–O bonds [44–46]. Thus, a few compositions among the $M^{II}M^{IV}(PO_4)_2$ ceramics investigated in the present work seems to be good candidates to meet the microwave applications requirements and should be further investigated in detail.

4. Conclusions

A series of double orthophosphates of $M^{II}M^{IV}(PO_4)_2$ type (M^{II} = Ca, Sr, Ba, Pb; M^{IV} = Ti, Zr, Hf, Ge, Sn) were prepared by solid state reaction method and consolidated by spark plasma sintering. The obtained ceramics are pure phases with high relative density. The permittivity at the frequency of 10^3 Hz is in the range of ~9.24 to ~42.56 for all the series of ceramic samples and the dielectric losses are small, in the range of ~0.01÷0.05. Low-frequency Maxwell–Wagner phenomena give important extrinsic contributions to the dielectric response of $BaZr(PO_4)_2$ (faint ionic conductor character), $BaTi(PO_4)_2$, $BaHf(PO_4)_2$ and $SrGe(PO_4)_2$, while the other compounds show typical Debye relaxation in kHz range. High-frequency dielectric investigations, in the range of frequency (10^6–10^9) Hz has revealed evidences that $SrGe(PO_4)_2$, $BaGe(PO_4)_2$, $CaZr(PO_4)_2$, $BaZr(PO_4)_2$, and $BaSn(PO_4)_2$ show excellent dielectric characteristics with small losses around 3÷6% and permittivities of 2.29÷8.02. The main reason of this behavior seems to be the lamellar structure of such compounds. Future work, will be directed, on the investigation of these double orthophosphate ceramics, because can be a promising material for use in microwave applications.

Acknowledgments

The authors would like to express their gratitude to Mr. Arnold Lacanilao for his technical support during SEM measurements. The dielectric characterization was performed within the RAMTECH centre under 162/15.06.2010 of POS CCE–A2-O2.1.2 grant. K.P. acknowledges City of Paris for the "Research in Paris" 2010–2011 fellowship.

References

[1] I.V. Tananaev, The Chemistry of Tetravalent Elements Phosphates , Nauka, Moskow, 1972.
[2] V. Brandel, N. Dacheux, J. Solid State Chem. 177 (2004) 4755.
[3] K. Popa, D. Bregiroux, R.J.M. Konings, T. Gouder, A.F. Popa, T. Geisler, P.E. Raison, J. Solid State Chem. 180 (2007) 2346.
[4] A.J. Locock, in: S.V. Krivovichev, P.C. Burns, I.G. Tananaev (Eds.), Stuctural Chemistry of Inorganic Actinide Compounds, Elsevier, Amsterdam, 2007.
[5] N. Clavier, R. Podor, N. Dacheux, J. Eur. Ceram. Soc. 31 (2011) 941.
[6] E. Morin, G. Wallez, S. Jaulmes, J.C. Couturier, M. Quarton, J. Solid State Chem. 137 (1998) 283.
[7] K. Fukuda, A. Moriyama, T. Iwata, J. Solid State Chem. 178 (2005) 2144.
[8] K. Fukuda, T. Iwata, A. Moriyama, S. Hashimoto, J. Solid State Chem. 179 (2006) 3870.
[9] D. Bregiroux, K. Popa, R. Jardin, P.E. Raison, G. Wallez, M. Quarton, M. Brunelli, C. Ferrero, R. Caciuffo, J. Solid State Chem. 182 (2009) 1115.
[10] D. Zhao, H. Zhang, Z. Xie, W.L. Zhang, S.L. Yang, W.D. Cheng, Dalton Trans. 27 (2009) 5310.
[11] K. Popa, G. Wallez, P.E. Raison, D. Bregiroux, C. Apostolidis, P. Lindqvist-Reis, R.J.M. Konings, Inorg. Chem. 49 (2010) 6904.
[12] G. Wallez, D. Bregiroux, K. Popa, P.E. Raison, C. Apostolidis, P. Lindqvist-Reis, R.J.M. Konings, A.F. Popa, Eur. J. Inorg. Chem. 1 (2011) 110.
[13] J. Xu, J. Zhang, J. Qian, J. Alloys Compd. 494 (2010) 319.
[14] L. Macalik, P.E. Tomaszewski, A. Matraszek, I. Szczygie, P. Solarz, P. Godlewska, M. Sobczyk, J. Hanuza, J. Alloys Compd. 509 (2011) 7458–7465.
[15] V. Venkatramu, R. Vijaya, S.F. Leon-Luis, P. Babu, C.K. Jayasankar, V. Lavin, L.J. Dhareshwar, J. Alloys Compd. 509 (2011) 5084–5089.
[16] G. Ju, Y. Hu, L. Chen, X. Wang, Z. Mu, H. Wu, F. Kang, J. Alloy Compd. 509 (2011) 5655–5659.
[17] G. Blasse, G.J. Dirksen, Chem. Phys. Lett. 62 (1979) 19.
[18] C.R. Miao, C.C. Torardi, J. Solid State Chem. 135 (2000) 229.
[19] Z.J. Zhang, J.L. Yuan, X.J. Wang, D.B. Xiong, H.H. Chen, J.T. Zhao, Y.B. Fu, Z.M. Qi, G.B. Zhang, C.S. Shi, J. Phys. D: Appl. Phys. 40 (2007) 1910.
[20] S. Arujan, B. Bhaskaran, R. Mohan Kumar, R. Mohan, R. Javavel, J. Alloys Compd. 506 (2010) 784.
[21] K. Popa, R.J.M. Konings, P. Boulet, D. Bouexiere, A.F. Popa, Thermochim. Acta 436 (2005) 51.
[22] K. Popa, R.J.M. Konings, O. Benes, T. Geisler, A.F. Popa, Thermochim. Acta 451 (2006) 1.
[23] D. Rose, Neues Jahrb. Mineral. Monatsh 247 (1980) 247.
[24] A. Tabuteau, M. Pages, J. Livet, C. Musikas, J. Mater. Sci. Lett. 7 (1988) 1315.
[25] R. Podor, M. Cuney, C. Nguyen Trung, Am. Miner. 80 (1995) 1261.
[26] J.M. Montel, J.L. Devidal, D. Avignant, Chem. Geol. 191 (2002) 89.
[27] K. Popa, T. Shvareva, L. Mazeina, E. Colineau, F. Wastin, R.J.M. Konings, A. Navrotsky, Am. Miner. 93 (2008) 1356.
[28] P.E. Raison, R. Jardin, D. Bouexiere, R.J.M. Konings, T. Geisler, C.C. Pavel, J. Rebizant, K. Popa, Phys. Chem. Miner. 35 (2009) 603.
[29] O. Terra, N. Dacheux, N. Clavier, R. Podor, F. Audubert, J. Am. Ceram. Soc. 91 (2008) 3673.
[30] I.S. Cho, J.R. Kim, D.W. Kim, K.S. Hong, J. Electroceram. 16 (2006) 379.

[31] K.R. Nair, P.P. Rao, B. Amina, M.R. Chandran, P. Koshy, Mater. Lett. 60 (2006) 1796.
[32] O.P. Shrivastava, N. Kumar, R. Chourasia, J. Mater. Sci. 42 (2007) 2551.
[33] M. Omori, Mater. Sci. Eng. A 287 (2000) 183.
[34] Z. Shen, Z. Zhao, H. Peng, M. Nygren, Nature 417 (2002) 266.
[35] M. Nygren, Z. Shen, Solid State Sci. 5 (2003) 125.
[36] N. Lupu, M. Grigoras, M. Lostun, H. Chiriac, J. Appl. Phys. 105 (2009), 07A738-07A738-3.
[37] R. Masse, A. Durif, C.R. Acad. Sci. Paris C 274 (1972) 108.
[38] I. Bunget, M. Popescu, Physics of Solid Dielectrics , Elsevier, New York, 1978.
[39] K. Amezawa, H. Maekawa, Y. Tomii, N. Yamamoto, Solid State Ionics 145 (2001) 233.
[40] J.P. Velev, P.A. Dowben, E.Y. Tsymbal, S.J. Jenkins, A.N. Caruso, Surf. Sci. Rep. 63 (2008) 400.
[41] H.M. O'Bryan, P.K. Gallagher, G.W. Berkstresser, C.D. Brandle, J. Mater. Res. 5 (1990) 183.
[42] K.P. Surendran, M.T. Sebastian, M.W. Manjusha, J. Philip, J. Appl. Phys. 98 (2005) 044101.
[43] C.L. Huang, Y.H. Chien, C.Y. Tai, C.Y. Huang, J. Alloys Compd. 509 (2011) L150–L152.
[44] J.J. Bian, D.W. Kim, K.S. Hong, Jpn. J. Appl. Phys. 43 (2004) 3521.
[45] I.S. Cho, H.S. Ryu, J.R. Kim, D.W. Kim, K.S. Hong, Jpn. J. Appl. Phys. 46 (2007) 2999.
[46] I.S. Cho, G.K. Choi, J.S. An, J.R. Kim, K.S. Hong, Mater. Res. Bull. 44 (2009) 173–178.